J Therm Anal Calorim (2014) 116:825–834
DOI 10.1007/s10973-013-3594-1

Oxidation properties of the Crofer 22 APU steel coated with $La_{0.6}Sr_{0.4}Co_{0.2}Fe_{0.8}O_3$ for IT-SOFC interconnect applications

Kazimierz Przybylski · Tomasz Brylewski · Ewa Durda · Richard Gawel · Andrzej Kruk

Received: 17 May 2013 / Accepted: 9 December 2013 / Published online: 30 January 2014

Abstract The $La_{0.6}Sr_{0.4}Co_{0.2}Fe_{0.8}O_3$ (LSCF48) cathode material was used as a protective-conducting coating on an interconnect made of Crofer 22 APU ferritic steel intended for application in intermediate-temperature solid oxide fuel cell (IT-SOFC) stacks. The LSCF48 coating was deposited on the surface of the steel via screen-printing followed by appropriate thermal treatment. The oxidation kinetics of the Crofer 22 APU steel—uncoated and coated with LSCF48—approximately obeys the parabolic rate law in air at 1,073 K under isothermal and cyclic oxidation conditions. The oxidation rate for uncoated steel is higher than that for coated steel. SEM–EDS and XRD investigations showed that the LSCF48 coating interacts with the steel during long-term oxidation in the afore-mentioned thermal conditions, and an intermediate multilayer interfacial zone is formed. This intermediate layer leads to lower area specific resistance in air at 1,073 K in comparison to the Crofer 22 APU steel without surface modification.

Keywords Solid oxide fuel cell (SOFC) · Oxidation kinetics · Metallic interconnects · Ferritic stainless steel · Cathode materials · Electrical resistance

Introduction

Solid Oxide Fuel Cells (SOFCs) are highly efficient devices which directly convert chemical energy from fuel gas to electrical energy by electrochemically oxidizing the fuel [1]. A key element that determines the functionality of a SOFC is its interconnect, which in an Interconnect-Supported Fuel Cell (ISFC) becomes the support element of the fuel cell [2]. The role of the interconnect is to ensure gas-tight separation between the cathode and anode compartments, and to provide electric contact between the units in a fuel cell stack and direct electrical energy to external devices. Furthermore, the above-mentioned fuel cell element must exhibit mechanical compatibility with adjacent electrodes as well as chemical stability [3].

Ferritic stainless steels (FSS) have been under consideration as potential metallic interconnect materials, because their thermal expansion coefficients (CTE) are comparable to those of SOFC electrodes, and they exhibit chemical stability in both oxidizing and reducing atmospheres [4–6]. The ferritic steel with the trade name 'Crofer 22 APU' was specifically designed as an interconnect material for SOFCs operating at temperatures below 1,173 K [3]. Other ferritic steels, such as JS 3 and Crofer 22 H (Thyssen Krupp VDM GmbH, Germany), ZMG (Hitachi Metals America, Ltd.), SUS 430 (Nippon Seisen Co., Ltd., Japan), and E-Brite (Allegheny Technologies Incorporated, USA), have also been specifically made for interconnect production, but Crofer 22 APU is currently the most studied. However, long-term corrosion and electrical resistance studies in air and H_2–H_2O gas mixture atmospheres have determined that despite exhibiting high resistance against oxidation due to the formation of a protective chromium oxide scale on the steel surface, the area specific resistance (ASR) of the steel/scale system gradually increases [4–7]. This is due to the low electrical conductivity of the Cr_2O_3 scale [7], the thickness of which increases according to the parabolic rate law [4]. Moreover, another disadvantage brought about by the scale is its

K. Przybylski (✉) · T. Brylewski · E. Durda · R. Gawel · A. Kruk
Faculty of Materials Science and Ceramics, AGH University of Science and Technology, Al. Mickiewicza 30, 30-059 Kraków, Poland
e-mail: kaz@agh.edu.pl

reactivity with the electrode material, especially on the air side of SOFC, which is the result of Cr species vaporization and diffusion into the cathode compartment [8]. The result of these phenomena is the degradation of the SOFC electrochemical performance, which, in turn, shortens the service life of the SOFC.

In order to inhibit these undesirable phenomena during long-term operation of a fuel cell stack in which each unit is separated by Crofer 22 APU interconnects, the surface of the steel is modified. This modification is carried out by depositing active protective-conducting coatings on the steel's surface [9, 10]. Many types of coating materials are in use, including $La_{0.9}Sr_{0.1}MnO_3$ [11], $La_{0.8}Sr_{0.2}CoO_3$ [12], Ag-perovskite [13], $(Mn,Co)_3O_4$ [14–16], and Y or Co [17, 18]. Such a modification makes it possible for the layered substrate made of corrosion-resistant steel and the protective-conductive coating to achieve low electrical surface resistance that does not change in time as well as high resistance to cyclic thermal oxidation and to effectively prevent chromium migration from the chromium-containing steel substrate.

A promising coating material for such applications is LSCF48, which has a perovskite structure and exhibits ionic and electronic conductivities that are both high at the same time [19, 20]. This material has been successfully used in IT-SOFC technology as a new generation cathode material [3, 9, 19]. Perovskite LSCF48 exhibits high chemical stability in the presence of yttria-stabilized zirconia (YSZ), which constitutes SOFC electrolyte material, desirable catalytic activity with regard to oxygen reduction in fuel cells operating in the temperature range of 873–1,073 K, and, furthermore, a thermal expansion coefficient that matches the coefficient of Crofer 22 APU [21]. Another advantage of this electrode is that it exhibits resistance to carbon deposition during oxidation in atmospheres containing methane [22, 23].

In this study, the surface of the Crofer 22 APU steel was coated with LSCF48 using screen-printing, followed by thermal treatment. The oxidation kinetics of uncoated and coated steel in air at 1,073 K under isothermal and cyclic oxidation conditions were studied. The phase composition, element distribution, and morphology of the oxidized Crofer 22 APU/LSCF48 composite were analyzed in detail. Additionally, the influence of the interface reactions between the ceramic coating and the steel substrate was discussed in terms of oxidation resistance and electrical properties.

Experimental

Preparation of study materials and oxidizing procedure

The material used for the experiments was the Crofer 22 APU ferritic stainless steel from ThyssenKrupp VDM GmBH, Germany. The chemical composition of this steel is presented in Table 1. Two types of samples were prepared for the purpose of the study: pure (i.e., uncoated) Crofer 22 APU steel and Crofer 22 APU steel with the LSCF48 coating. Samples in the shape of a rectangle with dimensions of about $10 \times 20 \times 1$ mm^3 were used for kinetic studies, while electrical resistance was measured using rectangular samples with dimensions of about $10 \times 10 \times 1$ mm^3. The surfaces of uncoated Crofer 22 APU specimens were ground with 100–1,200-grid SiC papers, then polished with a 0.3 μm alumina slurry (OP-U Struers, Denmark), ultrasonically degreased and finally washed in acetone immediately prior to each use. On the other hand, the steel substrate for the coating procedure was ground only with 600-grid SiC, after which it was cleaned using the method mentioned above.

The metallic substrate was coated with the LSCF48 paste using the screen-printing technique. The LSCF48 powder supplied by Marion Technologies (Toulouse, France) was used to prepare the paste. This powder had been prepared by the manufacturer via the calcination of a partially amorphous gel of co-precipitated hydroxides [24]. The paste was prepared by mixing the LSCF48 powder and a 5 mass% solution of ethyl cellulose in terpineol. The mixture, which contained ca. 17 mass% of organic binder, was homogenized. Thick films were deposited on the steel substrate, on surfaces abraded with a 120 mesh screen. The films were then dried for 2 h at 353 K. The coated Crofer 22 APU coupons were thermally annealed in air at a rate of 1 K min^{-1} to 1,073 K, which was then maintained for 1 h. The thickness of the coating was measured by means of microscopy, and it was determined to be in the 20−30 μm range.

Methods of sample characterization

Two thermal exposure testing procedures were applied in this work to study oxidation kinetics: continuous isothermal exposure testing, without intermediate cooling, and cyclic thermal oxidation testing, with repeated, regular and controlled temperature cycles. Continuous isothermal oxidation kinetics tests were performed in laboratory air at 1,073 K for a duration of 100 h using thermogravimetric equipment with the MK2 Vacuum Microbalance Head (CI Electronics Ltd., UK) with a sensitivity of 10^{-6} g. Cyclic thermal oxidation kinetics tests—including the measurement of net, gross and

Table 1 Chemical composition of Crofer 22 APU steel

Chemical composition/mass%							
Fe	Cr	Mn	Si	Ti	Al	Ni	La
Bal.	22.2	0.46	0.03	0.06	0.02	0.02	0.07

spall mass change—were carried out in laboratory air at 1,073 K for 528 h using equipment with a horizontal tube furnace, allowing the automatic configuration of the zone of maximum temperature of the furnace in relation to the samples placed in alumina crucibles in a quartz tube. Thermal cycles with a 24-h hot dwell time followed by rapid cooling in air were used. These investigations consisted of 22 cycles (1 cycle lasted 24 h). Before oxidation and after thermal cycles, each specimen and crucible was weighed with an accuracy of 10^{-5} g.

The phase composition of the products of oxidation of the pure and surface-modified steel was studied by means of X-ray diffraction (XRD) performed with a Philips Analytical X'Pert PW 3710 diffractometer, using monochromatic CuK_{α} radiation. The morphology and chemical composition of the oxidation products were investigated by means of scanning electron microscopy (SEM) performed using a FEI Nova NanoSEM 200 microscope coupled with an EDAX Genesis XM 2 system required for the analysis of chemical composition via energy-dispersive X-ray spectroscopy (EDS).

Electrical resistance measurements of the studied samples were conducted using complex impedance spectroscopic analysis (EIS). An impedance analyzer (AutoLab PGSTAT302N) was used over the frequency range from 1 mHz to 1 MHz. The temperature dependence of resistivity was measured in laboratory air at temperatures ranging from 473 to 1,073 K. The electrodes were composed of platinum. The ASR of the studied samples was calculated based on the obtained resistance values using the following formula:

$$\mathrm{ASR} = \frac{R \times S}{2} \tag{1}$$

where R is the electrical resistance (Ω), and S is the area of the Pt layer (cm^2).

Calculation of mass change during cyclic oxidation

Changes in sample mass during cyclic oxidation tests provide valuable data on the tendency of the scales formed on the surface of the investigated steels to spall and on the rate of their rehealing on exposed metal surfaces. To determine these changes, investigations of uncoated and coated Crofer 22 APU steel with LSCF48 were carried out in air at 1,073 K for 22 cycles (528 h). Based on the results, the net mass change (N) of the samples was determined with the following equation:

$$N = \frac{m_{\mathrm{ni}} - m_{\mathrm{n0}}}{A} \tag{2}$$

where m_{ni} is the mass of the sample after heating–cooling cycle i (g) and m_{n0} is the mass of the sample before heating–cooling cycle (g).

Furthermore, the total mass change of a given sample, scale and/or coating collected in a crucible (gross mass change—G) was determined as:

$$G = \frac{m_{\mathrm{gi}} - m_{\mathrm{g0}}}{A} \tag{3}$$

where m_{gi} is the total mass of the sample and crucible after heating–cooling cycle i (g) and m_{g0} is the total mass of the sample and crucible before the heating–cooling cycle (g).

The mass change of the scale and/or coating collected in the crucible (spall mass change—S) was calculated from the following equation:

$$S = G - N \tag{4}$$

Results and discussion

Oxidation kinetics of coated and uncoated Crofer 22 APU steel

Figure 1 shows the kinetics of isothermal oxidation of the uncoated and coated Crofer 22 APU steel with LSCF48, expressed as mass change (Fig. 1a) and squared mass change (Fig. 1b) in a function of time. These samples were oxidized in air at 1,073 K for 100 h. From Fig. 1, it follows that the oxidation kinetics of the studied samples approximately obey the parabolic rate law. The Pilling–Bedworth equation (5) was used to calculate the corresponding value of the parabolic rate constant (k_{p}) [25].

$$\left(\frac{\Delta m}{A}\right)^2 = k_{\mathrm{p}} \times t + \mathrm{C} \tag{5}$$

where $\Delta m/A$ is the mass gain per unit area (g cm^{-2}), k_{p} is the parabolic rate constant (g^2 cm^{-4} s^{-1}), t is the reaction time (s), and C is an integration constant defining the onset of parabolic kinetics.

The calculated parabolic rate constants for the oxidation of both studied samples at 1,073 K in air were of the order of 10^{-13}–10^{-14} g^2 cm^{-4} s^{-1}, typical of "*chromia formers*" [26, 27]. The oxidation rate of the Crofer 22 APU steel with the LSCF48 coating is 2.9×10^{-14} g^2 cm^{-4} s^{-1}, which is approximately one order of magnitude lower than the corrosion rate of the steel without surface modification (3.7×10^{-13} g^2 cm^{-4} s^{-1}). The research conducted, thus, far by other authors [28, 29] confirms that the screen-printed coating significantly inhibits oxide scale growth by reducing the supply of oxygen needed for the growth of chromia through the perovskite thick film (transport via oxygen vacancies).

Figure 2 presents the gross, nett and spall mass changes per 1 cm^2 of specimen surface during cyclic exposure of uncoated and coated Crofer 22 APU steel with LSCF48 in air at 1,073 K for an oxidation time of 528 h. From Fig. 2a,

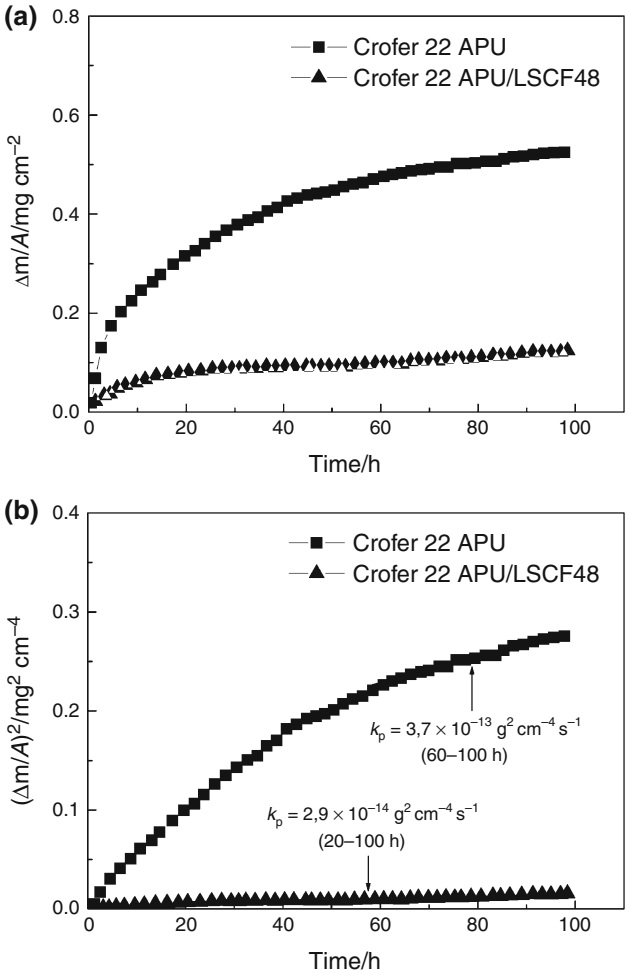

Fig. 1 Oxidation kinetics of Crofer 22 APU and Crofer 22 APU/LSCF48 samples in air for 100 h at 1,073 K expressed as mass change (**a**) and squared mass change (**b**) in a function of time (time intervals in which the parabolic rate law is obeyed are given in *parentheses*)

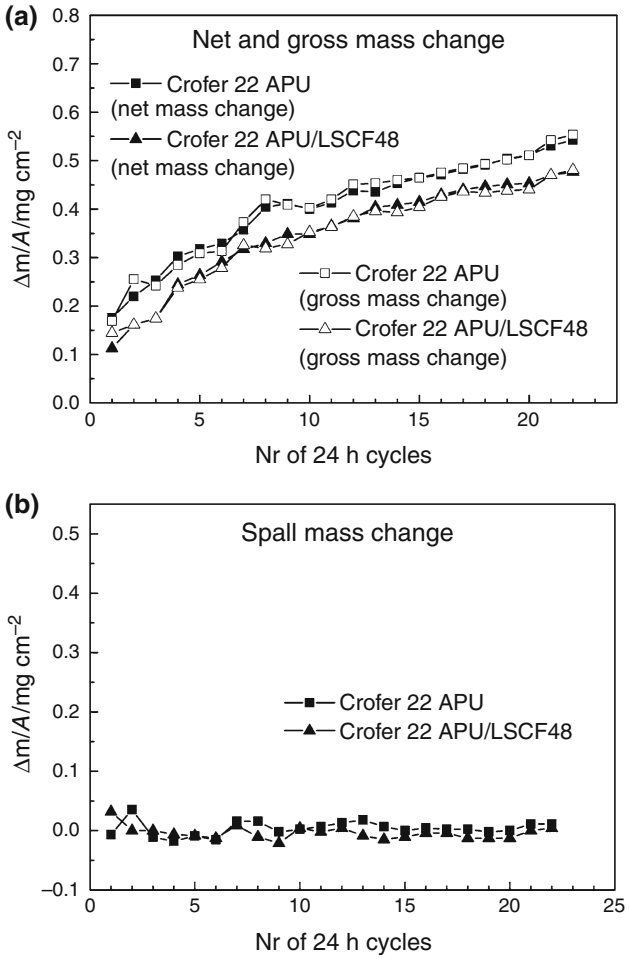

Fig. 2 Cyclic oxidation behavior of Crofer 22 APU and Crofer 22 APU/LSCF48 samples in air for 528 h at 1,073 K expressed as net and gross mass change (**a**), and spall mass change (**b**) in a function of time

it follows that the oxidation process of both studied samples approximately obeyed the parabolic rate law. This means that the slowest process which determines the rate of the oxidation process is the diffusion of the reactants in the scale or coating. For both the Crofer 22 APU steel without surface modifications and the Crofer 22 APU steel with LSCF48 coating, mass growth of the scale and/or coating collected in the crucible was small, although the coated steel exhibited a slight advantage in this respect (Fig. 2b). It can be concluded that the adhesion of both the scale and the LSCF48 coating to the metallic substrate during cyclic thermal oxidation testing was satisfactory. It is worth noting that the mass growth rate of the Crofer 22 APU steel sample expressed as net mass change is greater than the corrosion rate of the discussed steel with the LSCF48 coating (Fig. 2a), which is in accordance with the data on the oxidation kinetics of these samples obtained after tests in isothermal oxidation conditions (Fig. 1).

The above discussion of the results shows that the observed oxidation behavior demonstrated the beneficial role of the LSCF48 coating as a thermal protective coating for Crofer 22 APU in air at 1,073 K.

Microstructure and chemical composition of oxidation products formed on pure Crofer 22 APU steel and surface-modified steel

Figure 3 shows the X-ray diffraction patterns of the pure Crofer 22 APU steel and steel coated with LSCF48 oxidized in isothermal conditions in air at 1,073 K for 100 h. The scales formed on the surface of the pure Crofer 22 APU steel consist of Cr_2O_3 and a $MnCr_2O_4$ spinel phase. These results are consistent with those reported in [4, 30]. X-ray diffraction analysis of oxidation products in the Crofer 22 APU/LSCF48 composite revealed the presence of several phases, such as: $La_{0.8}Sr_{0.2}FeO_3$, $CoFe_2O_4$, $LaCrO_3$, Cr_2O_3, and $SrCrO_4$.

Figure 4 shows a comparison of X-ray diffraction patterns of the oxidation products formed on pure Crofer 22 APU steel and the Crofer 22 APU/LSCF48 composite after cyclic thermal oxidation testing in air at 1,073 K for 528 h. The same phases—i.e. Cr_2O_3 and $MnCr_2O_4$ in the pure Crofer 22 APU steel and $La_{0.8}Sr_{0.2}FeO_3$, $CoFe_2O_4$, $LaCrO_3$, Cr_2O_3, $SrCrO_4$ in the Crofer 22 APU/LSCF48—were obtained, as identified in the samples after isothermal oxidation.

Figure 5 presents the surface morphologies of the scales formed on the pure Crofer 22 APU steel after 100 h of isothermal oxidation (Fig. 5a) and 528 h of cyclic oxidation (Fig. 5b) in air at 1,073 K. SEM–EDS analyses of the scale formed on pure ferritic steel after isothermal oxidation revealed that the $MnCr_2O_4$ spinel phase had formed over the chromia scale, which was the main oxidation product (Fig. 5a). This spinel is present in the form of a thin, continuous outer layer, and linear precipitations along the grain boundaries of the steel, or visible "islets" in the form of well-developed grains. The diameter of these "islets" is in the range from around 1 μm to about 20 μm. The formation of chromium manganese spinel is caused by fast diffusion of manganese along the ferrite and chromia grain boundaries; on the surface, manganese reacts with the chromia that had initially formed and with the inwardly diffused oxygen anions to form the spinel phase [31]. The oxide scale formed on the studied steel exposed to cyclic

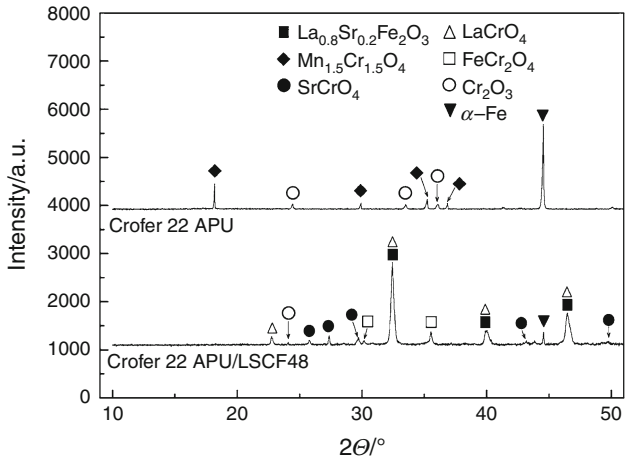

Fig. 3 X-ray diffraction patterns for Crofer 22 APU and Crofer 22 APU/LSCF48 samples, obtained after 100 h of isothermal oxidation at 1,073 K

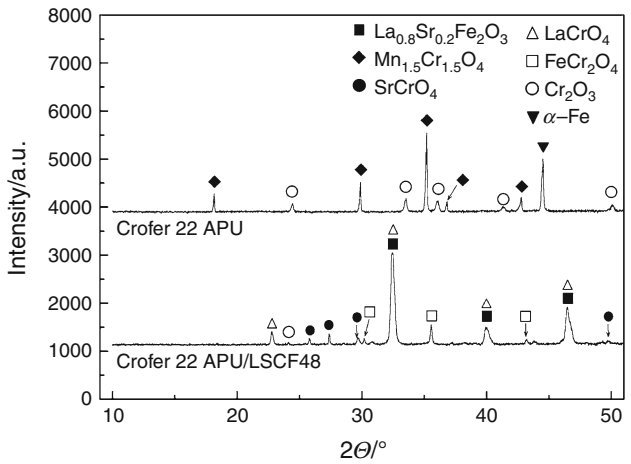

Fig. 4 X-ray diffraction patterns for Crofer 22 APU and Crofer 22 APU/LSCF48 samples, obtained after 528 h of cyclic oxidation at 1,073 K

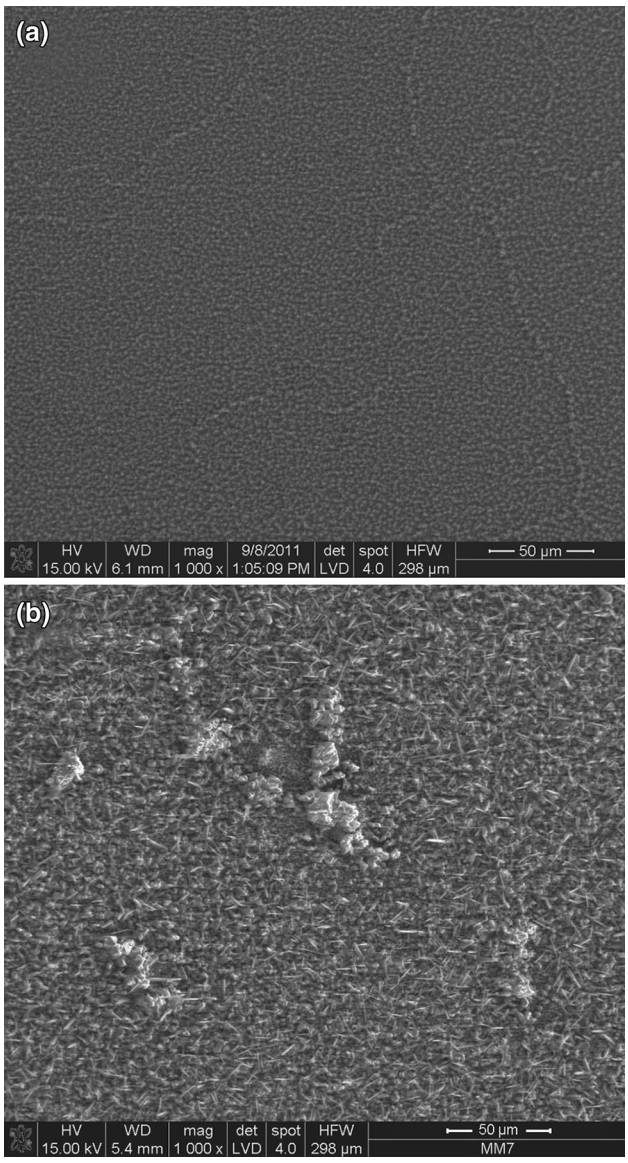

Fig. 5 SEM microphotographs of the surface of the scales formed on the Crofer 22 APU steel after 100 h of isothermal oxidation (**a**) and 528 h of cyclic oxidation (**b**) in air at 1,073 K

oxidation possesses a different microstructure. The surface of this scale is composed of well-defined Cr_2O_3 grains in the form of thin plates (Fig. 5b). Moreover, precipitates can be found between agglomerates of these grains. These precipitates consist of a large number of $MnCr_2O_4$ crystallites, which form local "islets" with sizes from 1 μm to 23 μm.

Figures 6 and 7 show the SEM microstructure of the polished cross-sections of the scales formed on the Crofer 22 APU steel after 100 h of isothermal oxidation (Fig. 6) and 528 h of cyclic oxidation in air at 1,073 K (Fig. 7). In both cases, the resulting scales are two-layer and consist of thick and continuous fine-crystalline inner layers built of chromia and a thinner outer layer consisting of the $MnCr_2O_4$ spinel. This is confirmed by means of XRD phase analysis (Figs. 3, 4) and chemical composition point analysis via EDS (regions 1 and 2). From Fig. 6, it follows that the scale is compact and adheres well to the metallic core. The average thickness of the Cr_2O_3 layer is about 3 μm, while that of the spinel layer is equal to about 0.5 μm. Scale thickness calculated from the parabolic oxidation rate constant corresponds to the average thickness of the scale estimated from the SEM morphology, within ±8 % (Fig. 6). The former value was calculated using the dependence:

$$x_s^2 = 2k_p \times t \tag{6}$$

Based on the relation between the thickness of the Cr_2O_3 scale and the mass change of the sample, determined during thermogravimetric measurements as [27].

$$\Delta m = x_s \times A \times \rho_{Cr_2O_3} \frac{3/2M_{O_2}}{M_{Cr_2O_3}} \tag{7}$$

where $\rho_{Cr_2O_3}$ is the density of chromia (g cm^{-3}), $M_{Cr_2O_3}$ is the molecular mass of the scale with Cr_2O_3 (g mol^{-1}), M_{O_2} is the molecular mass of oxygen (g mol^{-1}), and x_s is the thickness of scale layer (μm).

The scale formed on the surface of the Crofer 22 APU steel after 22 cycles of oxidation (Fig. 7) is compact and is characterized by poor adhesion to the metallic core compared to the scale formed on the steel after isothermal oxidation. In addition, the adhesion of the thin spinel layer to chromia is likewise unsatisfactory. This may be attributed to the effects of Cr_2O_3 and $MnCr_2O_4$ dilatation, which are the result of different thermal expansion coefficients of these oxides. Chemical analyses conducted at the steel/scale interface and within the metallic core revealed the presence of SiO_2 and Al_2O_3 precipitates (region 3). These oxides had formed as a result of internal oxidation of silicon and aluminum; the concentrations of these elements were higher than those found in region 4 corresponding to the steel. In addition, the same oxide precipitates were found in the case of the steel after isothermal oxidation (Fig. 6). The presence of these precipitates beneath the scale improves its adhesion to the substrate [26] and hinders the diffusion of chromium into the scale, thereby significantly reducing the rate of chromia growth on the Crofer 22 APU steel [32, 33].

Taking into account the fact that diffusion exchange may occur between the steel and the coating components during the operation of the steel/coating system in SOFC operation conditions, changes in the compositions of the material and protective coating should be expected in the vicinity of the steel/coating interface. As a result, an intermediate reaction layer is formed, the presence of which can significantly change the mechanical and electrical properties of the discussed system. Consequently, it

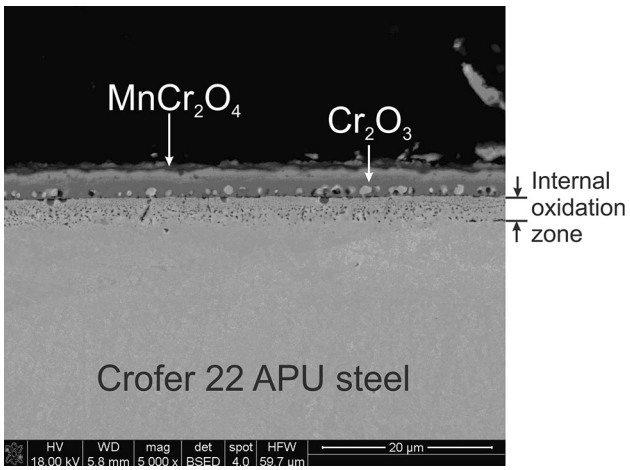

Fig. 6 SEM microphotograph of the polished cross-section of a scale formed on the Crofer 22 APU steel after 100 h of isothermal oxidation in air at 1,073 K

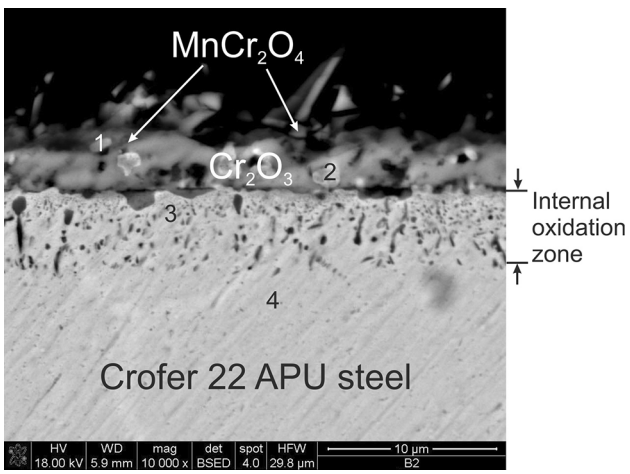

Fig. 7 SEM microphotograph of the polished cross-section of a scale formed on Crofer 22 APU steel after 528 h of cyclic oxidation in air at 1,073 K

is necessary to determine the morphology and chemical composition of this reaction layer.

Figure 8 shows the surface morphology of Crofer 22 APU coated with the LSCF48 thick film obtained via screen-printing after 100 h of isothermal oxidation (Fig. 8a) and 528 h of cyclic oxidation (Fig. 8b) in air at 1,073 K. Morphological observations using SEM have revealed that the external surface of the LSCF48 film oxidized in isothermal conditions is built of oval-shaped grains ranging from about 0.2–1 μm in size. After cyclic oxidation the size of regular grains in the form of agglomerates ranges from ca. 0.5 μm to about 1.5 μm.

Figure 9 shows SEM microphotographs of the cross-section of the Crofer 22 APU/LSCF48 composite after 100 h of isothermal oxidation (Fig. 9a) and 528 h of cyclic oxidation (Fig. 9b) in air at 1,073 K. The presented microphotographs demonstrate that the LSCF48 films obtained according to the above procedure exhibited good adhesion to the metallic core. Due to longer cyclic oxidation times, the studied oxide coating is significantly more porous compared to the same coating after isothermal oxidation. These films, which exhibit the similar thickness across the entire cross-section (≈25 μm), were built of oval grains. A common feature of the studied samples obtained after oxidation both in isothermal and cyclic conditions is the presence of an intermediate reaction layer at the steel/coating interface with a similar phase composition (Fig. 9), as shown by the X-ray diffraction patterns. The thickness of these intermediate reaction layers depends on oxidation conditions and ranges from about 1 μm to around 2 μm.

Detailed cross-sectional SEM–EDS and XRD investigations for the Crofer 22 APU/LSCF48 composite show that a compact multilayer consisting mainly of $CoFe_2O_4$, $SrCrO_4$, Cr_2O_3, $LaCrO_3$, and $La_{0.8}Sr_{0.2}FeO_3$ developed between the thick film and the steel substrate due to the simultaneous downward diffusion of cobalt and strontium from the LSCF48 coating material and upward diffusion of chromium and iron from the steel to the substrate/film interface (Fig. 10a). As can be seen from Fig. 10b, which shows the EDS line runs for La, Co, Sr, Cr, Fe, and O, performed along the white line of the boundary region, the intermediate layer was enriched with Co, Sr, Cr, Fe, and O. The increased Co, Fe, and O contents at the metal/scale

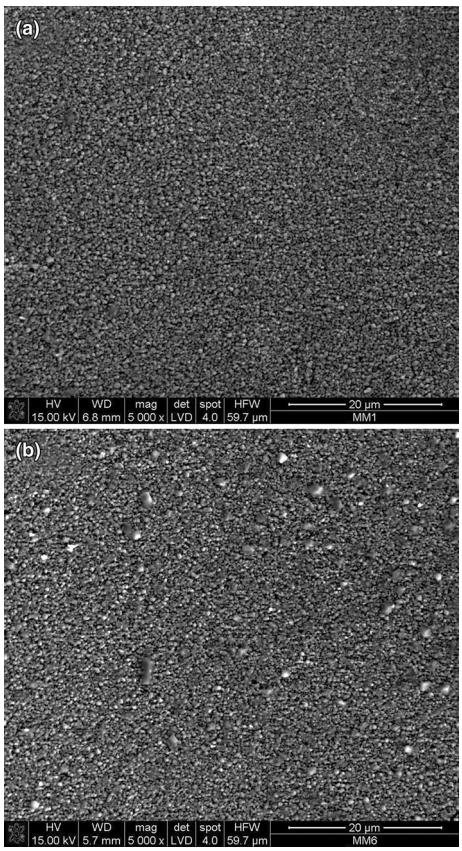

Fig. 8 SEM microphotograph of the surface morphology of LSFC48-coated Crofer 22 APU after 100 h of isothermal oxidation (**a**) and 528 h of cyclic oxidation (**b**) in air at 1,073 K

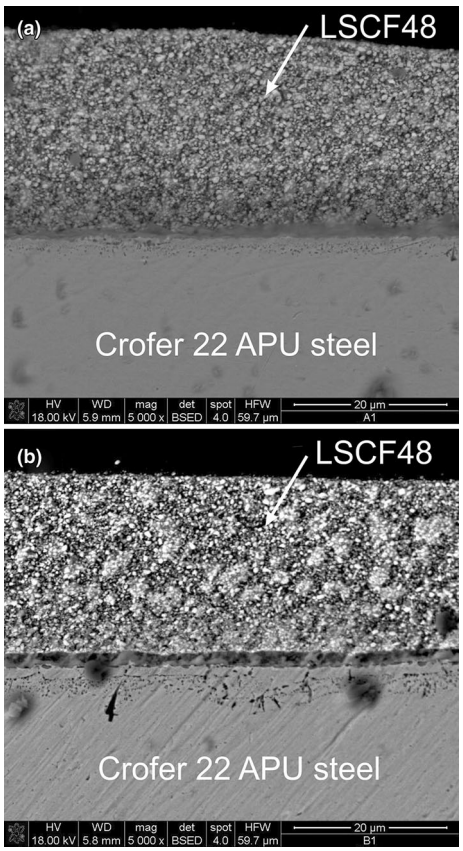

Fig. 9 SEM microphotograph of the polished cross-section of LSFC48-coated Crofer 22 APU after 100 h of isothermal oxidation (**a**) and 528 h of cyclic oxidation (**b**) in air at 1,073 K

interface may suggest the presence of a $CoFe_2O_4$ spinel layer, while the enrichment in Cr, Sr, and O observed at the upper part of the intermediate reaction layer corresponds to the formation of the $SrCrO_4$ and Cr_2O_3 phases. A similar effect of the LSCF48 perovskite coating was observed in studies by other authors [9, 34]. In some areas of the outer part of the afore-mentioned intermediate layer, the $LaCrO_3$ and $La_{0.8}Sr_{0.2}FeO_3$ perovskite phases developed as a result of the partial decomposition of the LSCF48 film through its reaction with the Cr_2O_3 and Fe_2O_3 oxides formed during initial oxidation on the steel surface, according to the simplified equation:

$$\begin{aligned} &La_{0.6}Sr_{0.4}Co_{0.2}Fe_{0.8}O_3 + 0.25\ Cr_2O_3 + 0.05\ Fe_2O_3 \\ &+ 0.1\ O_2 \rightarrow 0.2\ LaCrO_3 + 0.5\ La_{0.8}Sr_{0.2}FeO_3 \\ &+ 0.3\ SrCrO_4 + 0.2\ CoFe_2O_4 \end{aligned} \quad (8)$$

The presence of the phases included in the intermediate reaction layer was confirmed by performing XRD (Figs. 3, 4) and EDS (Fig. 10b) analyses. It should be noted that similar conclusions may be drawn from the morphology and chemical composition of the intermediate layer obtained after 528 h of cyclic oxidation of the Crofer 22 APU/LSCF48 composite material in air at 1,073 K.

Electrical properties of the oxidized pure Crofer 22 APU steel and surface-modified steel

In order to determine the electrical properties and evaluate the usefulness of the elaborated procedure for the fabrication of steel/coating composite materials used in the construction of metallic interconnects for IT-SOFCs, measurements of the ASR of the Crofer 22 APU/LSCF48 and pure Crofer 22 APU steel, for reference, were carried out using impedance spectroscopy. These measurements were performed in air over the temperature range of 473–1,073 K.

Figure 11 presents examples of impedance spectra registered at 473, 573, and 673 K for the Crofer 22 APU/LSCF48 composite after isothermal oxidation in air at 1,073 K for 100 h. A semicircle obtained at 473 K corresponds to a typical system consisting of a resistor (R_1) connected in series with another resistor (R_2) and a constant phase element (CPE) connected in parallel. However, at temperatures above 473 K, the presence of parasitic inductance produces significantly deformed shapes with positive imaginary values. This inductance occurs due to the high electrical conductivity of the sample at such temperatures. As temperature increases, the total resistance of all studied samples decreases, which indicates the electrical conductivity of a semiconductor. A similar temperature dependence of electrical resistance changes was determined in the case of pure Crofer 22 APU steel oxidized isothermally.

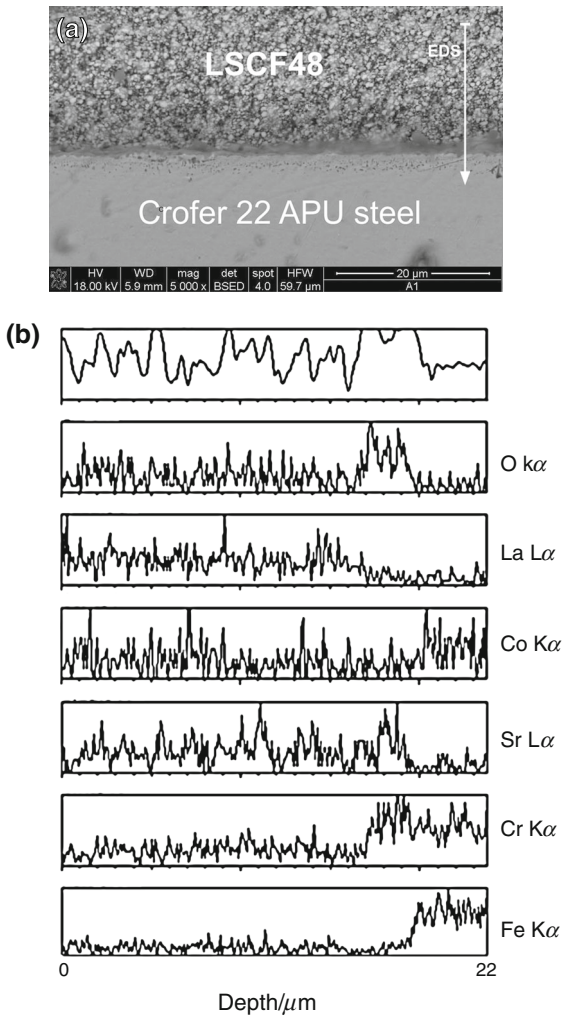

Fig. 10 SEM microphotograph of the polished cross-section of the Crofer 22 APU/LSCF48 composite after 100 h of isothermal oxidation in air at 1,073 K (**a**) and EDS line scan images (*across the line* shown in **b**) through the steel/coating interface

From the temperature dependence of ASR for the afore-mentioned samples, illustrated in Fig. 12, it can be concluded that, as temperature increases, the total resistance of the studied samples systematically decreases. The nature of these changes depends on the applied temperature range. At lower temperatures, i.e., in the range of 473–673 K, the surface modification of Crofer 22 APU steel is the key factor which determines the electrical conductivity of the studied samples. However, at temperatures above 673 K, the levels of electrical conductivity for the tested samples differ to a slight degree (see insets in Fig. 12). As shown in Fig. 12, at 1,073 K, the steel modified with the LSCF48 coating demonstrates an ASR at the level of 0.010 Ω cm^2, whereas for the pure Crofer 22 APU steel, the ASR is 0.0354 Ω cm^2, which is around 3.5 times higher than the value obtained for Crofer 22 APU/LSCF48. Both values

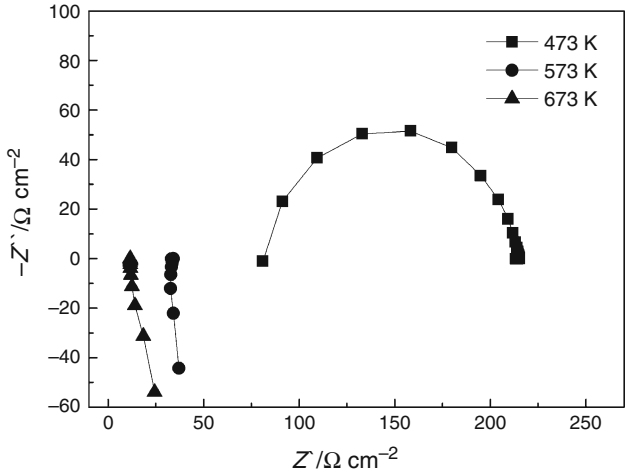

Fig. 11 Impedance diagrams of the Crofer 22 APU/LSCF48 composite measured at different temperatures

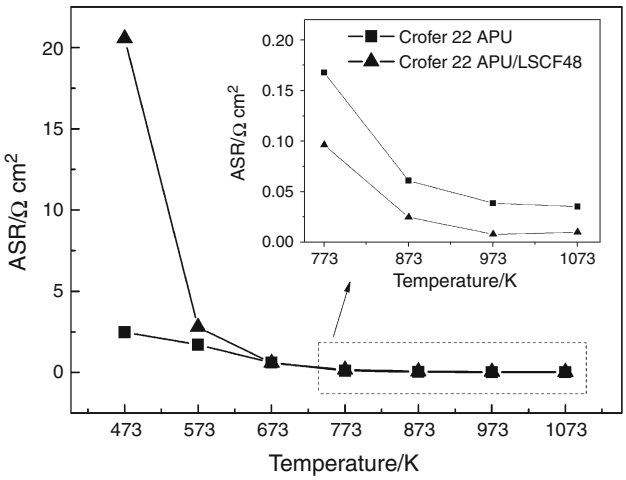

Fig. 12 Temperature dependence of ASR for the pure Crofer 22 APU steel and the Crofer 22 APU/LSCF48 composite

are well below the upper limit set for interconnect materials intended for SOFC application (0.1 Ω cm^2) [35]. The lower ASR value of the Crofer 22 APU/LSCF48 composite compared to the steel without surface modification is most likely due to the presence of a discontinuous chromia layer formed at the steel/coating interface as well as the effect of $SrCrO_4$ precipitation at the chromium oxide grain boundaries [5]. The influence of $SrCrO_4$ in equilibrium with Cr_2O_3 on conductivity is dependent on the temperature and partial pressure of oxygen, according to the following correlation [36]:

$$\sigma\left(\mathrm{S\ m^{-1}}\right) = 1.25 \times 10^{11} \exp\left(-\frac{220\ \mathrm{kJ\ mol^{-1}}}{RT}\right) \times p_{O_2}^{-5/12} \quad (9)$$

From Eq. (9), Chen et al. estimated the conductivity of $SrCrO_4$ in air at 1,073 K as 3.8×10^{-4} S cm^{-1} [37], which is lower than that of Cr_2O_3 (ca. 10^{-2} S cm^{-1}) [38]. However, a lower partial pressure of oxygen at the interface could have lead to a higher conductivity. The ASR values obtained for the Crofer 22 APU/LSCF48 composite in the present work were also lower than the values obtained in [9].

The observed results prove that the LSCF48 coating deposited on the Crofer 22 APU steel plays a protective role as a thermal and diffusion barrier against oxidation and chromium vaporization at 1,073 K in air, and that it is a promising candidate for chromia-forming metallic interconnects in planar IT-SOFCs.

Conclusions

A LSCF48 perovskite thick film on the Crofer 22 APU steel was fabricated using the screen-printing technique with a two-step procedure involving the deposition of paste on a metal substrate followed by heat-treatment in air. The oxidation kinetics of the Crofer 22 APU steel—uncoated and coated with LSCF48—approximately followed the parabolic rate law in air at 1,073 K in both isothermal and cyclic conditions. The oxidation rate for the steel coated with a perovskite thick film is lower than that for the uncoated steel, which indicates that the Crofer 22 APU/LSCF48 composite provides resistance against oxidation in the afore-mentioned conditions. The scales formed on the pure Crofer 22 APU steel after both isothermal and cyclic oxidation consisted mainly of a Cr_2O_3 layer and a $MnCr_2O_4$ spinel in the form of a thin external layer. The LSCF48 coating maintained good adhesion to the metal substrate after prolonged annealing during isothermal and cyclic oxidation. SEM–EDS investigations of the Crofer 22 APU/LSCF48 composite revealed the formation of an intermediate multilayer enriched with the $SrCrO_4$, $CoFe_2O_4$, Cr_2O_3, $LaCrO_3$, and $La_{0.8}Sr_{0.2}FeO_3$ phases between the coating and steel. ASR measurements of the Crofer 22 APU steel with and without surface modification, performed over the temperature range of 473–1,073 K, revealed semiconductor behavior. The Crofer 22 APU steel/LSCF48 composite shows lower electrical resistance compared to pure ferritic steel.

Acknowledgements The presented work was carried out as part of the statutory activities of the Department of Physical Chemistry and Modelling, Faculty of Materials Science and Ceramics, AGH University of Science and Technology (Contract No. 11.11.160.257). The authors are grateful to Dr. Jaroslaw Dabek for his assistance in thermogravimetric measurements.

References

1. Zeng Z, Natesan K. Corrosion of metallic interconnects for SOFC in fuel gases. Solid State Ionics. 2004;167:9–16.
2. Minh NQ. Solid oxide fuel cell technology—features and applications. Solid State Ionics. 2004;174:271–7.
3. Ardigò MR, Perron A, Combemale L, Heintz O, Caboche G, Chevalier S. Interface reactivity between $La_{0.6}Sr_{0.4}Co_{0.2}Fe_{0.8}O_{3-\delta}$ (LSCF) cathode material and metallic interconnect for fuel cell. J Power Sources. 2011;196:2037–45.
4. Fergus JW. Metallic interconnects for solid oxide fuel cells. Mater Sci Eng A. 2005;397:271–83.
5. Brylewski T, Nanko M, Maruyama T, Przybylski K. Application of Fe–16Cr ferritic alloy to interconnector for a solid oxide fuel cell. Solid State Ionics. 2001;143:131–40.
6. Brylewski T, Dabek J, Przybylski K. Oxidation kinetics study of the iron-based steel for solid oxide fuel cell application. J Therm Anal Calorim. 2004;77:207–16.
7. Kadowaki T, Shiomitsu T, Matsuda E, Nakagawa H, Tsuneizumi H, Maruyama T. Applicability of heat resisting alloys to the separator of planar type solid oxide fuel cell. Solid State Ionics. 1993;67:65–9.
8. Hilpert K, Das D, Miller M, Peck DH, Weib R. Chromium vapor species over solid oxide fuel cell interconnect materials and their potential for degradation processes. J Electrochem Soc. 1996;143:3642–7.
9. Tsai MJ, Chu CL, Lee S. $La_{0.6}Sr_{0.4}Co_{0.2}Fe_{0.8}O_3$ protective coatings for solid oxide fuel cell interconnect deposited by screen printing. J Alloys Compd. 2010;489:576–81.
10. Shaigan N, Qu W, Ivey DG, Chen W. A review of recent progress in coatings, surface modifications and alloy development for solid oxide fuel cell ferritic stainless steel interconnects. J Power Sources. 2010;195:1529–42.
11. Hwang H, Choi GM. The effects of LSM coating on 444 stainless steel as SOFC interconnect. J Electroceram. 2009;22:67–72.
12. de Silva ALA, Castro GGG, Souza MMVM. Synthesis of Sr-doped $LaCrO_3$ powders by combustion method. Influence of the fuel agent. J Therm Anal Calorim. 2012;109:33–8.
13. Wilkinson LT, Zhu JH. Ag-perovskite composite materials for SOFC cathode—interconnect contact. J Electrochem Soc. 2009;156:B905–12.
14. Choi JJ, Ryu J, Hahn BD, Yoon WH, Lee BK, Park DS. Dense spinel $MnCo_2O_4$ film coating by aerosol deposition on ferritic steel alloy for protection of chromic evaporation and low-conductivity scale formation. J Mater Sci. 2009;44:843–8.
15. Yang Z, Xia GG, Li XH, Stevenson JW. $(Mn, Co)_3O_4$ spinel coatings on ferritic stainless steels for SOFC interconnect applications. Int J Hydrogen Energy. 2007;32:3648–54.
16. Kruk A, Stygar M, Brylewski T. Mn–Co spinel protective-conductive coating on AL453 ferritic stainless steel for IT-SOFC interconnect applications. J Solid State Electrochem. 2013;17:993–1003.
17. Molin S, Kusz B, Gazda M, Jasinski P. Protective coatings for stainless steel for SOFC applications. J Solid State Electrochem. 2009;13:1695–700.
18. Chevalier S, Caboche G, Przybylski K, Brylewski T. Effect of nano-layered coatings on the electrical conductivity of oxide scale grown on ferritic steel. J Appl Electrochem. 2009;39:529–34.
19. Kournoutis VC, Tietz F, Bebelis S. AC impedance characterization of a $La_{0.8}Sr_{0.2}Co_{0.2}Fe_{0.8}O_{3-\delta}$ electrode. Fuel Cells. 2009;9:852–60.
20. Xu Q, Huang DP, Chen W, Lee JH, Wang H. Citrate method synthesis, characterization and mixed electronic-ionic conduction properties of $La_{0.6}Sr_{0.4}Co_{0.2}Fe_{0.8}O_3$ perovskite-type complex oxides. Scripta Mater. 2004;50:165–70.
21. Tai L-W, Nasrallah MM, Anderson HU, Sparlin DM, Sehlin SR. Structure and electrical properties of $La_{1-x}Sr_xCo_{1-y}Fe_yO_3$. Part 2. The system $La_{1-x}Sr_xCo_{0.2}Fe_{0.8}O_3$. Solid State Ionics. 1995;76:273–83.
22. Jin C, Liu J, Guo W, Zhang Y. Electrochemical characteristics of an $La_{0.6}Sr_{0.4}Co_{0.2}Fe_{0.8}O_3$–$La_{0.8}Sr_{0.2}MnO_3$ multilayer composite cathode for intermediate-temperature solid oxide fuel cells. J Power Sources. 2008;183:506–14.
23. Liu J, Co AC, Paulson S, Birss VI. Oxygen reduction at sol-gel derived $La_{0.8}Sr_{0.2}Co_{0.8}Fe_{0.2}O_3$ cathodes. Solid State Ionics. 2006;177:377–87.
24. Thorel AS. (Project coordinator). Periodic consortium report Y2 (D1.2). IDEAL-Cell project (2009).
25. Mrowec S, Werber T. Modern scaling-resistant materials. Washington DC: National of Standards and National Science Foundation; 1982.
26. Kofstad P. High temperature corrosion. London: Elsevier Applied Science Publishers Ltd.; 1988.
27. Birks N, Meier GH. Introduction to high temperature oxidations of metals. London: Edward Arnold Ltd.; 1983.
28. Yang Z, Xia G–G, Maupin GD, Stevenson JW. Conductive protection layers on oxidation resistant alloys for SOFC interconnect applications. Surf Coat Technol. 2006;201:4476–83.
29. Brylewski T, Dabek J, Przybylski K, Morgiel J, Rekas M. Screen-printed (La, Sr)CrO_3 coatings on ferritic stainless steel interconnect for solid oxide fuel cells using nanopowder prepared by means of ultrasonic spray pyrolysis. J Power Source. 2012;208:86–95.
30. Quadakkers WJ, Piron-Abellan J, Shemet V, Singheiser L. Metallic interconnectors for solid oxide fuel cells. Mater High Temp. 2003;20:115–27.
31. Cox MGE, Mc Enannay B, Scott VD. A chemical diffusion model for partitioning of transition elements in oxide scales on alloys. Philos Mag. 1972;26:839–51.
32. Atkinson A, Gardner JW. The diffusion of Fe^{3+} in amorphous SiO_2 and the protective properties of SiO_2 layers. Corros Sci. 1981;21:49–58.
33. Mikkelsen L, Linderoth S, Bilde-Sorensen JB. The effect of silicon addition on the high temperature oxidation of a Fe–Cr alloy. Mater Sci Forum. 2004;461–464:117–22.
34. Chou P-Y, Ciou C-J, Lee Y-C, Hung I-M. Effect of $La_{0.1}Sr_{0.9}Co_{0.5}Mn_{0.5}O_{3-\delta}$ protective coating layer on the performance of $La_{0.6}Sr_{0.4}Co_{0.8}Fe_{0.2}O_{3-\delta}$ solid oxide fuel cell cathode. J Power Sources. 2012;197:12–9.
35. Zhu WZ, Deevi SC. Development of interconnect materials for solid oxide fuel cells. Mater Sci Eng A. 2003;348:227–43.
36. Akashi T, Inoue T, Maruyama T. Electrical conductivity measurement for estimation of standard Gibbs energy change of ternary oxide formation. Mater Trans JIM. 2000;41:1646–50.
37. Chen L, Magdefrau N, Sun E, Yamanis J, Frame D, Burila C. Strontium transport and conductivity of $Mn_{1.5}Co_{1.5}O_4$ coated Haynes 230 and Crofer 22 APU under simulated solid oxide fuel cell condition. Solid State Ion. 2011;204–205:111–9.
38. Park J-H, Natesan K. Electronic transport in thermally grown Cr_2O_3. Oxid Met. 1990;33:31–54.